Icarus 199 (2009) 378–386

Contents lists available at ScienceDirect

Icarus

www.elsevier.com/locate/icarus

Three tenuous rings/arcs for three tiny moons

M.M. Hedman [a,*], C.D. Murray [b], N.J. Cooper [b], M.S. Tiscareno [a], K. Beurle [b], M.W. Evans [b], J.A. Burns [a,c]

[a] Department of Astronomy, Cornell University, Ithaca, NY 14853, USA
[b] Queen Mary University of London, Astronomy Unit, Mile End Road, London E1 4NS, United Kingdom
[c] Department of Theoretical and Applied Mechanics, Cornell University, Ithaca, NY 14853, USA

ARTICLE INFO

Article history:
Received 7 August 2008
Revised 6 November 2008
Accepted 10 November 2008
Available online 25 November 2008

Keywords:
Saturn, rings
Saturn, satellites
Resonances, rings

ABSTRACT

Using Cassini images, we examine the faint material along the orbits of Methone, Anthe and Pallene, three small moons that reside between the orbits of Mimas and Enceladus. A continuous ring of material covers the orbit of Pallene; it is visible at extremely high phase angles and appears to be localized vertically to within ±25 km of Pallene's inclined orbit. By contrast, the material associated with Anthe and Methone appears to lie in longitudinally confined arcs. The Methone arc extends over ~10° in longitude around the satellite's position, while the Anthe arc reaches ~20° in length. The extents of these arcs are consistent with their confinement by nearby corotation eccentricity resonances with Mimas. Anthe has even been observed to shift in longitude relative to its arc in the expected manner given the predicted librations of the moon.

1. Introduction

Since Cassini arrived at Saturn in the summer of 2004, it has made many discoveries—some are tangible, such as five new moons (Daphnis, Anthe, Methone, Pallene and Polydeuces) and several new rings, while others are conceptual, such as an improved understanding of the interaction between moons and nearby rings (e.g., Porco et al., 2007; Charnoz et al., 2007; Murray et al., 2008). The data described here can be counted among both of these sorts of discoveries: they are the first images of three previously unseen rings, but they also document novel relationships between small moons and low-optical-depth material.

The rings discussed here are localized near the orbits of Methone, Anthe and Pallene, three small moons of Saturn whose orbits lie between those of Mimas and Enceladus. The ability of such small moons to generate rings has been a subject of interest for some time (cf. Burns et al., 1999, 2004), and examples of faint rings interacting with similarly small moons have been found around all the giant planets: Jupiter (Burns et al., 1999, 2004; Showalter et al., 2007), Saturn (Porco et al., 2007; Murray et al., 2008), Uranus (Showalter and Lissauer, 2006) and Neptune (de Pater et al., 2005). However, evidence that these particular saturnian moons do in fact produce faint rings has only recently become available. Images of a ring associated with Pallene, charged-particle absorptions ascribed to material near Methone, and images of arcs associated with both Anthe and Methone were announced in the last two years (Porco et al., 2006a; Roussos et al., 2006; Porco et al., 2008).

After reviewing prior in situ evidence for material associated with at least one of these moons, this paper will describe the structure of the rings associated with Pallene, Methone and Anthe as they have been observed by Cassini's cameras. After this, we discuss of how the variety of structures seen in these rings can be understood in terms of the detailed dynamical environments of the relevant moons. Note that this paper does not consider here the faint ring which lies near the orbits of Janus and Epimetheus (Porco et al., 2006a). These moons' much larger masses and their unique co-orbital resonant configuration make the dynamics of their ring a special case that is beyond the scope of this paper.

2. Previous detections of material associated with Methone

Before discussing the images of these rings, we must first mention the in situ measurements of charged particle absorptions that provided the earliest evidence for dispersed material associated with these moons. Historically, charged particle absorption signatures have often provided the first hints of low-optical depth rings. For example, Jupiter's ring was first suggested when Pioneer 10 detected low energetic-particle fluxes inwards of Amalthea's orbit (Acuna and Ness, 1976) and Saturn's G ring was detected through its modest reduction in several species of charged particles as measured by Pioneer 11 (cf. van Allen, 1983). In both these cases subsequent imaging confirmed the existence of rings in these locations. More recently, a combination of in situ and remote-sensing data of the arc in the G ring yielded a consistent model for the origin of this ring (Hedman et al., 2007). However, there are

* Corresponding author.
E-mail address: mmhedman@astro.cornell.edu (M.M. Hedman).

0019-1035/$ – see front matter
doi:10.1016/j.icarus.2008.11.001

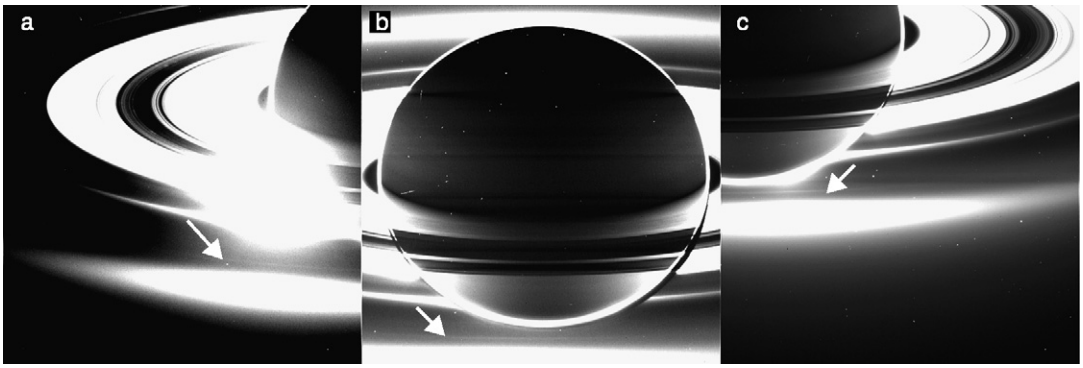

Fig. 1. Representative images of the Pallene ring obtained during the Day 258 of 2006 eclipse observations: (a) W1537005302 from the HIPHASE001 sequence; (b) W1537028814 from the HIPHWAC001 sequence; (c) W1537050260 from the HIPHASE002 sequence. All images were taken with the Wide-Angle Camera (WAC) using the VIO filter. The brightness scales are individually stretched for presentation. These three images were obtained at 9:23, 15:55 and 21:52 UTC, respectively. In all three images the Pallene ringlet (marked with an arrow) is most visible just off Saturn's southern limb, where the phase angle is highest.

also instances (Chenette and Stone, 1983; Cuzzi and Burns, 1988; Jones et al., 2008; Kerr, 2008) where the connection between the in situ measurements and visible rings is more uncertain and controversial.

The in situ measurements relevant to this work consist of two absorption signatures of ~MeV-electrons that have been identified in three channels of MIMI/LEMMS data obtained very close to Methone's L-shell (i.e. where magnetic field lines threading the spacecraft pass close to Methone's orbit). These absorptions occurred when the satellite was "upstream" and longitudinally nearby the magnetic field lines connected to the spacecraft (Roussos et al., 2008). The inbound and outbound microsignatures are each tens of percent deep and have radial extents of 2400 km and 1500 km, respectively. The inbound signature was separated by 17° from Methone and lay nearly 5000 km exterior to Methone's L-shell, whereas the outbound depletion was separated by about 5° from Methone and occurred exactly on the satellite's L-shell. Because Methone is so small and inert, by itself the moon is not likely to generate a >1000-km wide signature. Roussos et al. (2008) instead investigate the possibility of a dust arc, treating it in the manner of Cuzzi and Burns (1988). They conclude that a 15°-long arc comprised of particles larger than a mm and with an optical depth lower than the E or G rings ($\sim 10^{-6}$) would provide a sufficient obstacle to account for the observed absorption. As described below, imaging data now confirm such material does in fact exist around Methone.

The radial shift of the inbound detection relative to Methone's L-shell is not easily explained (Roussos et al., 2008). This shift results in the absorption occurring closer to Anthe's L-shell, so an arc of material in that moon's orbit could possibly explain that absorption. However, the images discussed below show that the material associated with Methone and Anthe are organized into longitudinally-confined arcs 10–20 degrees across. Anthe was over 120° from Cassini when these absorptions were observed, and while microsignature identification can be a complex problem, we think it is more likely that both signatures are due to Methone. We may also note in passing that there are other cases, notably including the G-ring arc detection (Hedman et al., 2007), where similarly puzzling radial displacements are seen.

3. Imaging observations

The images discussed here were obtained by the Imaging Science Subsystem (ISS) onboard the Cassini spacecraft. This consists of a Narrow-Angle Camera (NAC) and Wide-Angle Camera (WAC), each of which is equipped with multiple color filters (Porco et al., 2004). All images are initially processed using the CISSCAL calibration routines (Porco et al., 2004) that remove backgrounds, flatfield the images, and convert the raw data numbers into I/F, a standardized measure of reflectance. I is the intensity of the scattered radiation while πF is the solar flux at Saturn, so I/F is a unitless quantity that equals unity for a perfect Lambert surface viewed at normal incidence. Note that these automated routines do not eliminate all instrumental artifacts in the images, and so additional processing is often needed to extract information about faint features like those discussed here.

In order to facilitate comparisons between observations taken from different elevation angles, we often convert the observed I/F values to "normal I/F" $= \mu I/F$, where μ is the cosine of the emission angle. The normal I/F should be independent of emission angle so long as $\tau/\mu \ll 1$ (where τ is the ring's normal optical depth) and the ring opening angle is sufficiently high that the vertical width of the ring can be neglected. While the former is certainly true for these faint rings, the latter condition is likely violated in some of the nearly edge-on images.

The images containing the Pallene ring happen to have been taken at extremely high phase angles (>175°) or extremely low ring opening angles (<0.5°), while the images containing the Methone and Anthe rings are at relatively low phase angles (<50°). We therefore will consider the Pallene ring observations separately from those of the Anthe and Methone rings below.

3.1. Pallene ring

The Pallene ring is seen most clearly in images obtained by Cassini on Day 258 of 2006, when the spacecraft flew through Saturn's shadow and was therefore permitted to observe the rings at extremely high phase angles (>175°). While the cameras obtained images through a number of different filters, we will only consider here the images taken through the short-wavelength VIO filter (effective central wavelength 420 nm). These images are the most useful for studying the morphology of faint structures like the Pallene ring because various artifacts due to scattered light in the optics are least prominent at these wavelengths. Furthermore, these images are the least likely to exhibit "bleeding" due to hyper-saturation of the image on the bright limb of the planet. The images taken through the VIO-filter therefore provide us with the "cleanest" pictures of the Pallene ring. (Images from other filters will be used in a later paper describing the spectrophotometric properties of such faint rings.)

Fig. 1 shows representative VIO-filter images taken during this time period. All these images show a bright ring with a full-width at half-maximum of approximately 2500 km located roughly 212,000 km from Saturn's center, near the orbit of Pallene. This ringlet is only clearly visible above the background in these images at phase angles above 178°, so the full longitudinal extent of

Table 1
High-phase, VIO filter images of the Pallene ring discussed in this paper.[a]

Filename	Image midtime	Exposure (s)	Phase angle	Emission angle	Longitude of Pallene	Visibility
			Rev 28 HIPHASE001			
W1537005302	2006-258T09:23:17	3.2	>175°	74°	342.3°	V
			Rev 28 HIPHWAC001			
W1537028438	2006-258T15:48:53	3.2	>175°	75°	65.3°	V
W1537028814	2006-258T15:55:09	3.2	>175°	75°	66.7°	V
W1537029190	2006-258T16:01:25	3.2	>175°	75°	68.0°	V
			Rev 28 HIPHASE002			
W1537050260	2006-258T21:52:32	10	>175°	74°	143.8°	V
W1537050679	2006-258T21:59:31	10	>175°	74°	145.3°	V
W1537051098	2006-258T22:06:30	10	>175°	74°	146.8°	V
W1537051517	2006-258T22:13:29	10	>175°	74°	148.3°	V
W1537051936	2006-258T22:20:03	10	>175°	74°	149.9°	V
W1537052355	2006-258T22:27:27	10	>175°	74°	143.4°	V

[a] The longitudes of the moons reported are measured in an inertial coordinate system tied to J2000. The longitude range (found in Tables 3 and 4) is the total range of longitude in the relevant moon's orbit covered by the image. Under the Visibility column: "V" means the ring/arc is visible, "F" means ring/arc visible but very faint, "S" means the image of the arc is highly smeared and "?" means that it is not clear if the ring is visible.

Table 2
Clear-filter NAC images of the region around Pallene.[a]

Rev	Filename	Image midtime	Exposure (s)	Phase angle	Emission angle	Longitude of Pallene	Visibility
019	N1514138009	2005-358T17:24:10	4.6	86.7°	90.3°	201.6°	V
046	N1560588018	2007-166T08:05:49	32	42.8°	89.5°	188.8°	?
048	N1563638697	2007-201T15:29:51	68	167°	90.0°	45.6°	V
048	N1563638854	2007-201T15:32:28	68	167°	90.0°	46.1°	V
061	N1584374445	2008-076T15:23:35	32	18.9°	80.0°	50.6°	?
063	N1586003593	2008-095T11:55:45	46	13.7°	85.9°	174.9°	?

[a] See tablenote of Table 1.

this ring cannot be determined from any single image. Fortunately, this feature was observed in three separate imaging sequences (HIPHASE001, HIPHWAC001 and HIPHASE002; see Table 1). The available images of the Pallene ring cover an interval of approximately twelve hours or about one-half of Pallene's orbital period, and therefore can be used to constrain longitudinal variations in this ring's density.

To reliably compare the data from the different sequences, we need to account for the variations in the phase angle within the various images. We therefore computed phase curves for the Pallene ring from each of the three different observing sequences using the following procedure: First, we re-project each image onto a radius-longitude grid, and compute the observed phase angle for each point in this grid. The data are then sorted into a series of 0.1°-wide bins in phase angle and the data within each bin are averaged together to produce a series of radial brightness profiles. For each radial profile, we fit a cubic to the data interior and exterior to the Pallene ringlet and subtract this background from the profile. We then integrate over radius to determine the so-called equivalent width of the ringlet in each profile:

$$\text{equivalent width} = \int (\mu I/F)\, dr. \quad (1)$$

(In this case the integral covered a radial range of 9000 km centered on the orbit of Pallene.) This quantity has units of length and is a measure of the total integrated brightness of the ring (it also has the advantage that it should be independent of the image resolution). Equivalent widths from different images within the same sequence are averaged together to produce a single series of brightness measurements versus phase angle for each sequence (Fig. 2). For the HIPHASE002 sequence, only data at phase angles above 178.8° are presented because at lower phase angles a camera artifact (consisting of a dark horizontal band) obscures the Pallene ring.

While the shapes of these phase curves are sensitive to the particle size distribution of the Pallene ring, such detailed photometric

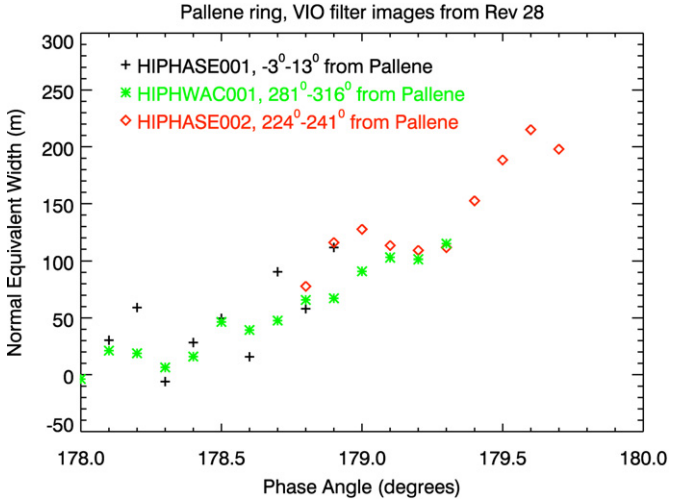

Fig. 2. Phase curves for the Pallene ringlet derived from the three eclipse observation sequences illustrated in Fig. 1. Note that the three phase curves match wherever they overlap, which suggests that the density of material does not depend strongly on longitude relative to Pallene.

analyses are beyond the scope of the present paper. For the purposes of this analysis, it is only important to note that wherever two curves overlap in phase angle, they give roughly the same value for the total integrated brightness of the Pallene ring. This implies that there are not gross variations in the ring's density or particle size distribution between three sections of the ring. Since these three parts of the ring are separated from Pallene by 5°, 62°, and 128° in longitude, this feature must extend over at least one-third of Pallene's orbit, and is therefore probably a truly continuous ring (unlike the features associated with Anthe and Methone, discussed below).

We have also searched for evidence of the Pallene ring in images outside of this particular extremely high-phase opportunity. Given the faintness of this feature, it is most likely to be detectable

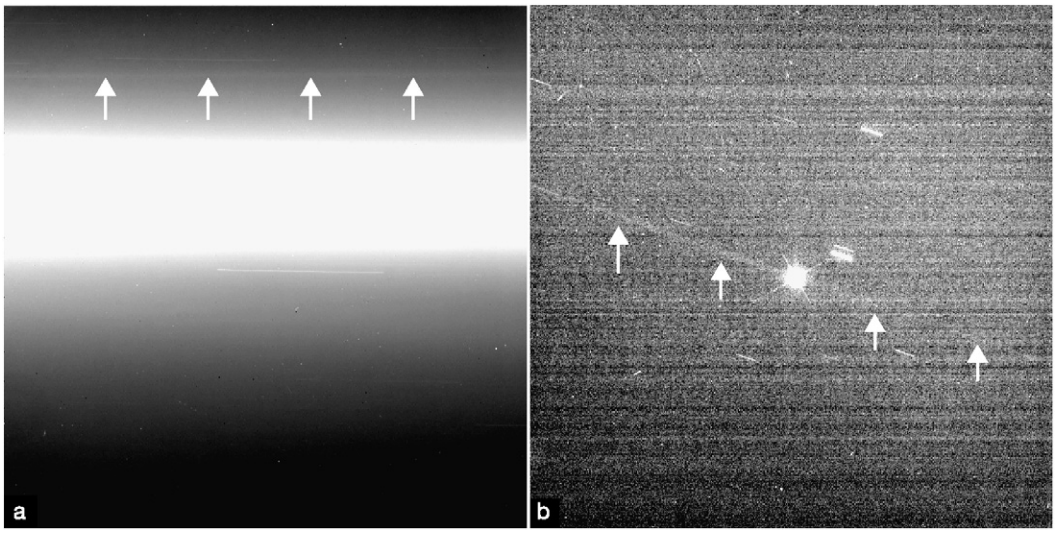

Fig. 3. Nearly edge-on views of the Pallene ring at moderate to high phase angles: (a) N1563638697, phase angle of 167°, ring opening angle of 0.02°; (b) N1514138009, phase angle of 87°, ring opening angle of 0.26°. Both images are rotated so that Saturn's north pole would point approximately up, and are individually stretched. The Pallene ring is marked with white arrows in both images. Note the bright band near the center of image (a) corresponds to the G ring, and the bright spot in the center of image (b) is Pallene itself. In image (a) Pallene falls off the left edge of the frame at roughly the same height above the ringplane as the marked feature. Orbital motion is from left to right in both images.

in images with long exposure times when the spacecraft was close to the ringplane. Only NAC images were searched because artifacts due to stray light in the instrument are typically much better for the NAC than for the WAC, especially at higher phase angles. Furthermore, it is useful to have Pallene in or near the field of view to confirm the relationship between any observed feature and this moon. Table 2 is a list of (NAC clear-filter) images with exposure times greater than 1 s and opening angles less than 10° that were taken near Pallene. Among these images, those obtained at phase angles below 80° do not yield clear detections of the Pallene ring. While some suspicious features in these images could be related to this ring, it is currently difficult to determine if they are real structures or simply camera artifacts. This is in contrast to the Methone and Anthe rings, which can be reliably discerned in images taken with comparable exposure times and viewing geometries. This may be because the Pallene ring is significantly broader than the arcs associated with Anthe and Methone, which makes it more difficult to pick out in these images. It is also possible that the Pallene ring is less backscattering than either the Anthe or Methone ring arcs.

The Pallene ring can be detected in two sets of images acquired at phase angles above 80° and ring opening angles less than 0.5°. One set of images was taken on Day 201 of 2007, when Cassini observed the rings at high phase angles while the spacecraft passed through the ringplane. Due to the finite inclination of its orbit, Pallene was located well above the ringplane during a part of this sequence. Two images of the region near this moon (one of which is shown in Fig. 3a) reveal a faint streak lying at the same distance above the ringplane as Pallene; almost certainly this represents the Pallene ringlet. Another image containing the Pallene ringlet was obtained on Day 358 of 2005 (see Fig. 3b). This image was targeted at Pallene but the exposure time was sufficiently long and the ring opening angle was sufficiently low to detect the Pallene ring as a very faint streak that passes obliquely through the moon. As in the previous images, both Pallene and the ring are shifted vertically in these images due to their finite orbital inclinations.

Given the extremely low ring opening angles of both these observations, the apparent widths of the ring in these images place strong constraints on its vertical height. Both these observations indicate that this ring is extremely thin, having an approximately Gaussian vertical profile with a full-width at half-maximum of less than 50 km. This is much less than the ~1300 km vertical excursions of the moon from Saturn's equatorial plane. The particles is this ring are therefore tightly clustered about Pallene's orbit. This is in contrast to the Jovian gossamer rings which are also associated with small inclined moons, but have vertical extents comparable to the vertical excursions of their parent moons (Burns et al., 2004, and references therein). However, recent images of the gossamer ring associated with Amalthea reveal a component in this ring that is tightly confined to the orbital plane of its parent moon (Fig. 15 in Showalter et al., 2008). This feature may be analogous to the observed Pallene ring.

3.2. Anthe and Methone ring arcs

Unlike the Pallene ring, which was first noticed in extremely high phase-angle images (Porco et al., 2006b), the low optical-depth material associated with Methone and Anthe was first recognized in a series of low-phase images obtained on Day 302 of 2007 (Porco et al., 2008; see Table 3). These images were part of an observation intended to recover Anthe using the preliminary orbit determination available at the time. It was designed and implemented within four days of Anthe's discovery on Day 173 of 2007. If this observation had simply been intended for satellite astrometry, exposure durations of 0.68 s would have been selected, and the ring arcs would not have been detectable. However, since this observation was designed to recover a newly discovered satellite, five of the images have long (15 s) exposures to assure that this object would be obvious if detected.

Fig. 4a shows one of these images after processing by the standard calibration pipeline. Both Anthe and Methone are present in this image (indicated by black and white arrows, respectively). Two faint, narrow arcs surrounding these moons can barely be seen above the remaining background variations in the image. Both these structures are visible in all five of the long-exposure images, and at least the Anthe arc (which is near the maximum elongation of Anthe's orbit) has the curvature one would expect for a ring's ansa. These features therefore appear to be real and not artifacts.

In order to better characterize these structures, we needed to further reduce the background variations. In particular, we wished to lessen the residual horizontal banding in the images (Porco et al., 2004). To accomplish this, we fit a quadratic to each row of brightness measurements and subtracted this background from the

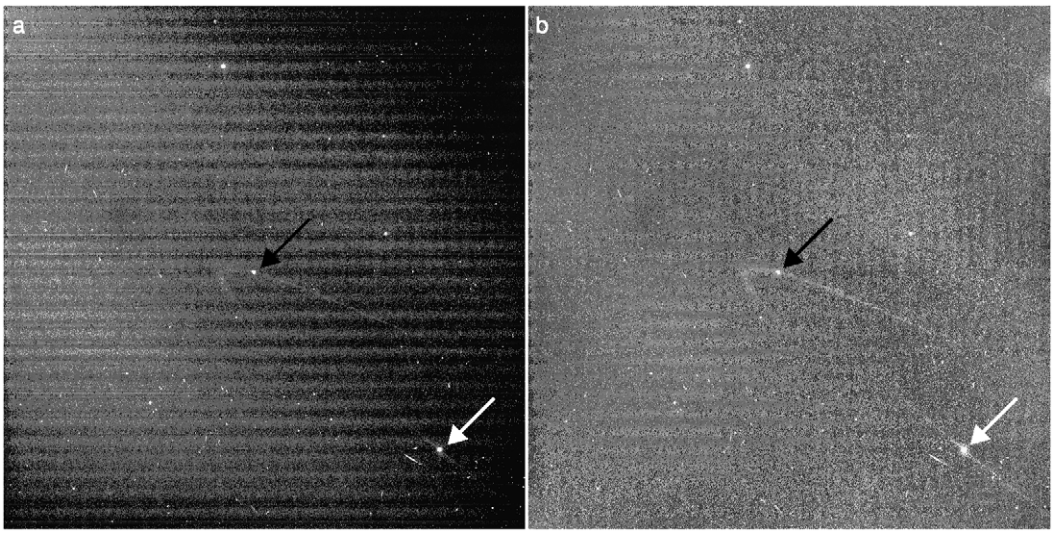

Fig. 4. One of the images (N1582353098) taken on Day 302 of 2007, that first revealed the Anthe arc and the Methone arc to the remote-sensing instruments: (a) The image after standard calibration and flat-fielding, (b) the same image after additional removal of a quadratic background from each line (see text). In both images, Anthe is marked with a black arrow and Methone with a white arrow. The faint streaks surrounding these moons are the Anthe and Methone arcs. Orbital motion is clockwise.

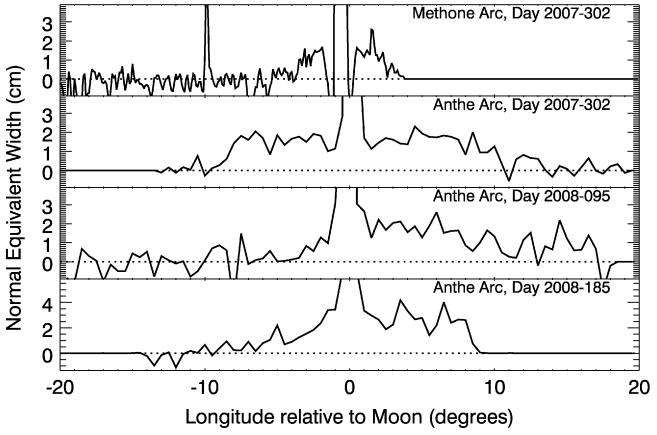

Fig. 5. Longitudinal profiles of the Methone (top) and Anthe arcs derived from the two image sequences illustrated in Figs. 4, 6, and 8. The spike at the center of all the profiles is due to the embedded moon. Note that the dips on either side of the central spike in the top profile are artifacts introduced by the background-subtraction algorithm.

data. As can be seen in Fig. 4b, this procedure greatly reduced the banding but did not affect the signal from the arcs.

These images clearly show that this material does not form continuous rings at the orbit of the moon, but instead extends only a finite range of longitudes around their parent moons. To better quantify the brightness and longitudinal extent of these arcs, we re-projected each of the five images onto a radius-longitude grid and for each longitude bin we computed the equivalent width of the arc above the remaining background using Eq. (1). (In this case, the integration was done over a radial zone 600 km wide centered on the apparent radial position of the relevant moon.) These integrated brightness measurements were then binned in longitude relative to the moon to create the first two profiles displayed in Fig. 5. These profiles show that both the Methone and Anthe arcs have a peak normal equivalent widths of between 1 and 2 cm at a phase angle of 23°, and that both arcs extend roughly the same distance ahead and behind their parent moons. The Methone arc only covers 10° in longitude, while the Anthe arc is larger, extending over nearly 20° in longitude.

After this sighting of the arcs, we searched for earlier images of these features, again focusing on images containing the relevant moons that had long exposure times and low ring opening angles. Also, after this discovery some subsequent images targeted at Anthe, Methone and Pallene were designed to have very long exposures in an effort to recover these arcs. Tables 3 and 4 list all the images obtained thus far where we can see the Anthe and Methone arcs. As expected, the arcs are easier to identify at low ring opening angles. However, it is somewhat surprising that all of the available images of the arcs are at low phase angles. By contrast, low-elevation high-phase images containing Anthe (e.g., N1516296328) do not show any evidence for a bright feature near the orbit of this moon. Even the extremely high-phase images that revealed the Pallene ring (see Fig. 1) do not provide clear evidence for concentrations of material near the orbits of Methone or Anthe. Unfortunately, it is difficult to evaluate the significance of this non-detection. Unlike the orbit of Pallene, which lies just outside Saturn's limb, the orbits of both Anthe and Methone actually pass in front of Saturn's disk in these extremely high-phase images. Thus the rings would be most detectable at the point where they emerge from the planet's limb, and here it is most difficult to isolate real ring features from various instrumental artifacts.

Many of the low-phase observations of the Methone and Anthe arcs taken before or after the images from Day 302 of 2007 only cover a very limited range of longitudes ($<10°$) around the moon and/or have low signal-to-noise. They therefore can provide little additional information about the structure and evolution of these arcs. The exceptions to this are two sets of three images of the Anthe arc obtained on Days 95 and 185 of 2008.

The images from Day 95 (see Fig. 6) show Anthe and the arc near maximum elongation and capture all or most of the longitudinal extent of the arc. Furthermore, these images have significantly higher signal to noise than the earlier images of the arc, and so reveal previously unseen substructures in this arc. In Figs. 6a and 6b, a dark channel can be seen running down the middle of the arc, just ahead of the moon. This substructure becomes clearer when the imaging data are re-projected onto a grid of radii and longitudes relative to Anthe (see Fig. 7). In this format, we can see that in all three images the arc has the same basic structure. Between 0° and 5° ahead of Anthe, the arc has a distinctly "double-stranded" appearance, with an outer strand lying close to the same radial position as the moon and the inner strand lying roughly 200 km closer to the planet. Both strands become more diffuse and likely merge together with increasing distance from

Table 3
Known clear-filter NAC images of the Anthe arc.[a]

Rev	Filename	Image midtime	Exposure (s)	Phase angle	Emission angle	Longitude of Anthe	Longitude range	Visibility
046	N1560618365	2007-166T16:31:48	8.2	44.3°	89.5°	119.7°	<10°	V
051	N1572352978	2007-302T12:07:22	15	22.6°	88.4°	128.0°	~30°	V
051	N1572353038	2007-302T12:08:22	15	22.6°	88.4°	128.3°	~30°	V
051	N1572353098	2007-302T12:09:22	15	22.6°	88.4°	128.5°	~30°	V
051	N1572353158	2007-302T12:10:22	15	22.6°	88.4°	128.7°	~30°	V
051	N1572353218	2007-302T12:11:22	15	22.6°	88.4°	129.0°	~30°	V
051	N1572353442	2007-302T12:15:12	2.6	22.6°	88.4°	129.9°	~30°	F
059	N1582636683	2008-056T12:41:05	32	27.7°	71.3°	65.8°	<10°	F
061	N1583627560	2008-067T23:55:38	32	33.8°	66.4°	88.8°	<10°	V
063	N1585394528	2008-088T10:44:51	32	31.4°	66.5°	352.6°	<10°	F
063	N1585438613	2008-088T22:59:36	32	42.1°	56.9°	169.3°	<10°	F
063	N1586002250	2008-095T11:33:28	32	23.4°	86.8°	275.4°	~30°	V
063	N1586003083	2008-095T11:47:15	46	23.4°	86.6°	279.2°	~20°	V
063	N1586004500	2008-095T12:10:59	32	23.3°	86.4°	284.5°	~30°	V
071	N1591878680	2008-163T11:53:05	56	9.7°	92.1°	142.7°	<10°	V
074	N1593748425	2008-185T03:15:32	26	11.5°	88.0°	98.6°	<10°	V
074	N1593753319	2008-185T04:37:03	32	11.8°	87.2°	118.3°	~20°	V
074	N1593758213	2008-185T05:58:40	26	12.8°	86.4°	138.0°	<10°	V

[a] See tablenote of Table 1.

Table 4
Known clear-filter NAC images of the Methone arc.[a]

Rev	Filename	Image midtime	Exposure (s)	Phase angle	Emission angle	Longitude of Methone	Longitude range	Visibility
045	N1559320893	2007-151T16:04:48	320	41.6°	84.2°	4.5°	<10°	S
051	N1572352978	2007-302T12:07:22	15	22.6°	88.4°	144.7°	~30°	V
051	N1572353038	2007-302T12:08:22	15	22.6°	88.4°	144.9°	~30°	V
051	N1572353098	2007-302T12:09:22	15	22.6°	88.4°	145.2°	~30°	V
051	N1572353158	2007-302T12:10:22	15	22.6°	88.4°	145.4°	~30°	V
051	N1572353218	2007-302T12:11:22	15	22.6°	88.4°	145.7°	~30°	V
051	N1572353442	2007-302T12:15:12	2.6	22.6°	88.4°	146.6°	~30°	F
060	N1582719964	2008-057T11:49:06	32	35.3°	65.5°	95.0°	<10°	F
060	N1583324168	2008-064T11:39:06	32	10.4°	88.8°	69.1°	<10°	V
061	N1583757191	2008-069T11:56:06	32	41.8°	59.5°	56.5°	<10°	F
061	N1584374115	2008-076T15:18:05	32	20.6°	77.4°	82.9°	<10°	F
063	N1585394198	2008-088T10:39:21	32	32.2°	65.9°	333.9°	<10°	F
063	N1586002693	2008-095T11:40:44	46	30.9°	87.0°	325.6°	<10°	V

[a] See tablenote of Table 1.

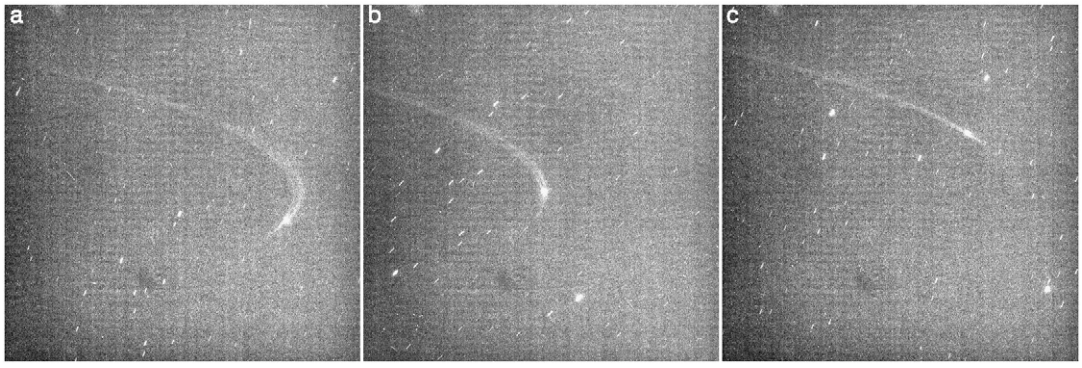

Fig. 6. A sequence of three images of the Anthe arc obtained on Day 95 of 2008: (a) N1586002250, (b) N1586003083, (c) N1586004500. All have been rotated so that Saturn's north pole would point upwards. The moon and the arc move through maximum elongation during this sequence of images in a counterclockwise direction. Note that substructure in the arc is visible in all of these images.

the moon. The inner strand actually appears to bend outward to join the main strand near Anthe.

The images from Day 185 are shown in Fig. 8. While all three images clearly show the arc, the middle image (Fig. 8b), again obtained when Anthe was near its maximum elongation, covers the largest range of longitudes, including the trailing end of the arc (unfortunately, the leading end of the arc was not captured in the field of view). A re-projected version of this image is provided in Fig. 8d for comparison with the Day 95 observations. Note that the arc does not appear to be "double-stranded" at this time.

An interesting aspect of all these later images is that the arc no longer appears to be centered on the moon. As with the previous images, we process the data from the reprojected images shown in Figs. 7 and 8 to obtain longitudinal profiles of the Anthe arc (see Fig. 5). These data show that the integrated brightness of the arc did not change significantly between the first two observations, which were both obtained at phase angles of ~23°. The arc appears somewhat brighter in the Day 185 observations, but these data were obtained at lower phase angles (~12°), so this is probably a photometric effect. In both the observations that captured

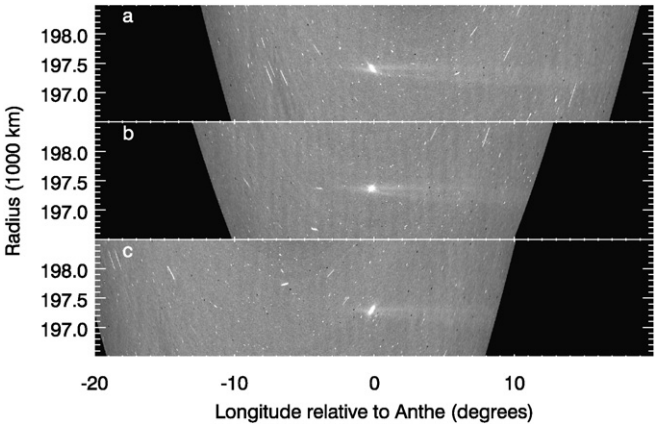

Fig. 7. Reprojected versions of the same images of the Anthe arc shown in Fig. 6: (a) N1586002250, (b) N1586003083, (c) N1586004500. The imaging data are displayed here as functions of radius and longitude relative to Anthe in order to facilitate comparisons between the different data sets; orbital motion is from left to right. The substructure of the arc is much easier to see in this format. Note in particular the "double-stranded" appearance of the arc just to the right of Anthe.

the entire arc, its total length is ∼20°. However, it appears that the arc shifted between 5° and 10° forward in longitude relative to the moon between Day 302 of 2007 and Day 95 of 2008. We can understand this phenomena in terms of the detailed dynamical environment of this moon and arc, as discussed in Section 4.

4. Dynamical considerations

All of the rings and arcs discussed above are likely generated by debris knocked off of the nearby small moons. Depending on their surface properties and their radial location, small satellites (5 km to 50 km) can be ideal sources to supply debris for a ring since they present a reasonably large cross-section to be struck by micrometeoroids, but they have little gravity to hold onto any impact ejecta (Burns et al., 1999).

The morphology of the low-optical-depth material associated with these small moons shows surprising diversity. Pallene appears to share its orbit with a nearly continuous ring of material that is most visible at high phase angles, while Methone and Anthe are both embedded in arcs of limited longitudinal extents that have thus far only been seen at low phase angles. The arc associated with Anthe even appears to drift in longitude relative to its parent moon. It turns out that the gross features of these rings and arcs can be explained in terms of the detailed dynamical environments of the three moons.

Keep in mind that, within the three-body problem, the orbital region near any moon is not particularly stable, and particles will drift longitudinally through Kepler shear, at least as long as they lie beyond the satellite's Hill sphere. To state this differently, the only longitudinally trapped material in the three-body problem outside the moon's Hill sphere lies on stable tadpole and horseshoe orbits that, respectively, encompass (loop around) the triangular points (L4 or L5) or circumambulate three libration points (L3, L4 and L5) on each pass. However, particles can be confined in an arc due to resonances with more distant satellites, as seen with Saturn's G-ring arc (Hedman et al., 2007) or Neptune's ring arcs (Porco, 1991). If the satellite is itself near to or trapped in a resonance with some neighboring satellite, some debris may be ejected onto circumplanetary orbits that are trapped in the same resonant well.

While Methone, Anthe and Pallene all orbit Saturn between Mimas and Enceladus, they occupy distinct dynamical environments.

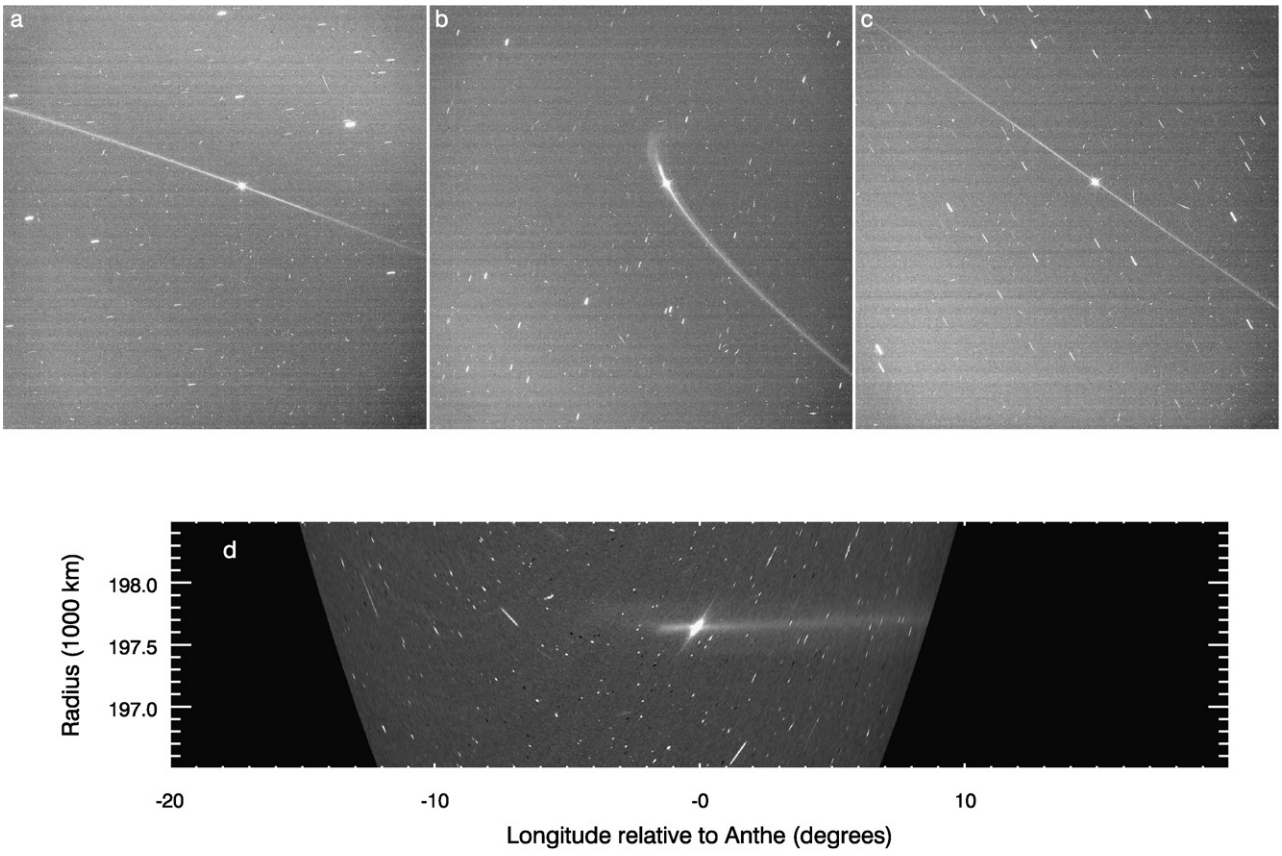

Fig. 8. Observations of the Anthe arc obtained on Day 185 of 2008. The top row is the three images in this sequence: (a) N1593748425, (b) N1593753319, (c) N1593758213. Anthe is moving to the left in (a), downwards in (b) and to the right in (c). Panel (d) shows the middle image re-projected as a function of radius and longitude relative to Anthe, for comparison with Fig. 7.

Existing numerical integrations indicate that both Methone (Spitale et al., 2006) and Anthe (Cooper et al., 2008) are trapped in first-order mean-motion resonances with Mimas. By contrast, Pallene is not near any strong first-order resonance, although it may librate about a third-order resonance with Enceladus (Spitale et al., 2006). This suggests that nearby resonances with Mimas may be confining material from Anthe and Methone in longitude to produce discrete arcs, while material from Pallene is free to spread over all longitudes to form a complete ring.

Further evidence for a connection between nearby resonances and the morphology of these faint rings can be found by analyzing the relevant resonant arguments. For example, one of the librating resonant arguments of Anthe (Cooper et al., 2008) is

$$\phi = 11\lambda_{\text{Anthe}} - 10\lambda_{\text{Mimas}} - \varpi_{\text{Mimas}}. \quad (2)$$

Anthe therefore occupies the 11:10 corotation eccentricity resonance with Mimas. Corotation eccentricity resonances are able to confine ring material in longitude, especially when the optical depth of the material is sufficiently low that inter-particle collisions can be neglected (Goldreich et al., 1986; Porco, 1991; Namouni and Porco, 2002; Hedman et al., 2007). This resonance therefore provides a natural explanation for the existence of the Anthe arc.

The longitudinal extent of the Anthe arc is consistent with this confinement mechanism. An 11:10 resonance produces 11 evenly-spaced stable longitudes around which material can be trapped. Material librating around these stable points therefore will form an arc that is at most $360°/11 = 32°$ across. The arc associated with Anthe is 20° long, well below this limit. Note that the G-ring arc similarly covers a smaller longitudinal range than the maximum possible for a resonantly trapped population (Hedman et al., 2007).

Even the observed motion of the arc relative to Anthe between Day 302 of 2007 and Day 95 of 2008 is consistent with this model. Fig. 9 plots the residual longitude of Anthe relative to a constant mean motion of 347.349°/day based on numerical integrations of Anthe's orbit (Cooper et al., 2008), and thus illustrates how Anthe librates in longitude relative to the stable points of the 11:10 corotation eccentricity resonance. This graph reveals that on Day 302 of 2007, Anthe was near the stable point, while on Days 95 and 185 it was approximately 5° behind the stable point. The arc's motion relative to the moon can therefore be explained as follows: the arc consists of many particles librating around the 11:10 corotation resonance and so the arc as a whole moves around the planet at the same rate as this resonance. Anthe (as the largest member of this swarm) also librates around this resonance but between Day 302 of 2007 and Day 95 of 2008, it drifted backwards through this resonance and therefore it shifted towards the trailing end of the arc. Indeed, the relative motion of the moon through the arc during this time may have been responsible for scattering some of this material to produce the inner strand visible in Day 95 of 2008. Between Days 95 and 185 of 2008 Anthe turned around, so while it still lags behind the arc, it is now moving forwards through the arc. We therefore expect that some future observations will show the arc's center lagging behind Anthe.

The libration of Anthe within this resonance may even help explain the "double stranded" appearance of Anthe on Day 95 of 2008. For example, the inner strand of the arc may be composed of particles that have been scattered by a close encounter with Anthe as the moon moved through the arc. Another possibility is that the particles in the arc were launched at such low velocities from Anthe that the particles actually trace out the path of the moon through the corotation zone. Numerical simulations are underway to investigate these issues (Agarwal et al., 2008).

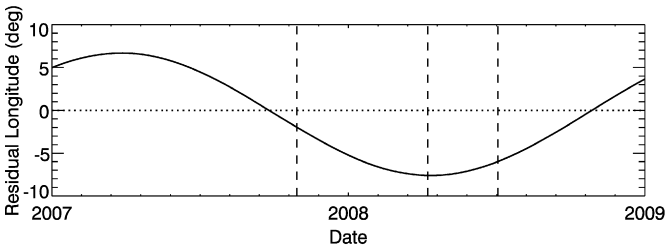

Fig. 9. The libration of Anthe's longitude around a stable point of the 11:10 corotation eccentricity resonance with Mimas. This plot shows the numerically-integrated residual longitude of Anthe relative to a constant mean motion of 347.349°/day. The three vertical lines correspond to the times when the arc was observed (Day 302 of 2007, Day 95 of 2008 and Day 185 of 2008, from left to right).

The situation for the Methone arc is less clear. Spitale et al. (2006) detected a libration in the resonant argument:

$$\phi = 15\lambda_{\text{Methone}} - 14\lambda_{\text{Mimas}} - \varpi_{\text{Methone}}, \quad (3)$$

which would mean that Methone occupies the 15:14 outer Lindblad resonance with Mimas. However, it turns out that these same integrations show that another argument also librates:

$$\phi = 15\lambda_{\text{Methone}} - 14\lambda_{\text{Mimas}} - \varpi_{\text{Mimas}}. \quad (4)$$

This corresponds to the 15:14 corotation eccentricity resonance with Mimas. Methone therefore appears to occupy both of these resonances, which are separated by less than 4 km in semi-major axis. The dynamics of Methone are therefore rather complicated. However, the 15:14 corotation eccentricity resonance could potentially be responsible for confining the Methone arc. The longitudinal extent of the arc is only 10°, significantly less than the maximum possible $360°/15 = 24°$, which is consistent with such a model.

Unfortunately, since the full extent of the arc was only observed on Day 302 of 2007, we are not yet able to determine if this arc moves relative to Methone in a manner consistent with a resonantly trapped population. In fact, the numerical integrations indicate that on Day 302 of 2007, Methone's longitude should have been roughly 5° behind the longitude of the stable point. This suggests that Methone should have been near the trailing end of its arc, not at its center, as observed. (However, the leading edge of this arc lies near the edge of the field of view, so its extent in that direction could be underestimated.) Thus, while it is likely that the corotation eccentricity resonance plays some role in confining Methone's arc, a detailed understanding of the dynamics of this region will require additional simulations and observations.

Given the importance of corotation eccentricity resonances in maintaining the Anthe and possibly the Methone arcs, these structures can be regarded as variants of the G ring arc where the largest fragment (that is, the moon) is visible. Furthermore, the ability of these arcs to absorb energetic particles and their visibility at low phase angles implies that they contain relatively large particles (>100 μm), like the G ring arc. Indeed, it is possible that Anthe could eventually give rise to another G ring. If Anthe were disrupted by a sufficiently large impact, some amount of the detritus from this collision would likely remain trapped in the resonance. The greatly increased surface area of this debris would strongly enhance the production of dust in this resonance, yielding a much brighter arc and possibly even a complete ring as smaller particles drift outwards due to various drag forces.

5. Conclusions and prospects

The rings and arcs associated with these small moons provide yet more opportunities to investigate the complex interactions between moons and ring particles. While the elementary considera-

tions discussed above can provide reasonable qualitative explanations for the gross morphology of these faint arcs and rings, more much more work needs to be done in order to fully understand the dynamics of these systems. Numerical simulations of these systems are underway (Agarwal et al., 2008) and will be presented in a future paper.

For example, it is remarkable that the Pallene ring appears to be concentrated about the inclined orbit of the satellite, implying that the nodal longitudes of the individual particles are aligned. Differential precession of particle orbits with different semi-major axes is expected to cause the nodes to become randomized, producing a vertically extended torus like Jupiter's gossamer rings (Burns et al., 2004, and references therein). Perhaps the particles in the Pallene ring do not survive long enough (because of various erosion processes) for their nodes to become randomized. If so, then one could place constraints on the dispersion in the semi-major axes and/or the lifetime of these particles (Agarwal et al., 2008). Note that Jupiter's Amalthea ring also displays a bright concentration of material near its source moon (Showalter et al., 2008) despite the moon's inclination, so these phenomena may be observable here as well.

The detailed morphology of the Anthe arc also requires further investigation and detailed modeling. The structures seen in Figs. 6 and 7 bear a striking resemblence to the so-called "tendrils" observed in the diffuse material near Enceladus, the E ring source (Porco et al., 2006b). Comparisons between these two systems may well be productive.

Besides the morphological differences among these extremely faint rings, there is also some evidence for differences in their photometric properties, in that the Anthe and Methone arcs have only been seen at low phase angles and the Pallene ring has only been seen at high phase angles. While this may simply be an artifact of the sparseness of the currently available data, this could also reflect differences in the particle size distribution which in turn may reflect differences in how particles are liberated from the moons' surfaces. More detailed photometric analyses are needed to evaluate such possibilities.

Acknowledgments

We wish to thank the Imaging Team and the Cassini Project for their support of this work. J.A.B., M.M.H. and M.S.T. also acknowledge support from NASA's Planetary Geology and Geophysics program. C.D.M., M.W.E., K.B. and N.J.C. acknowledge the financial support of the UK Science and Technology Facilities Council. We want to thank R. Jacobson for discussions about the Methone resonance. We also thank S. Charnoz and M. Showalter for their helpful comments.

References

Acuna, M.J., Ness, N.F., 1976. The main magnetic field of Jupiter. J. Geophys. Res. 81, 2917–2922.

Agarwal, M., Tiscareno, M.S., Hedman, M.M., Burns, J.A., 2008. Dynamics of faint rings associated with Methone, Anthe and Pallene. In: AAS/Division for Planetary Sciences Meeting Abstracts, vol. 40, p. 30.02.

Burns, J.A., Showalter, M.R., Hamilton, D.P., Nicholson, P.D., de Pater, I., Ockert-Bell, M.E., Thomas, P.C., 1999. The formation of Jupiter's faint rings. Science 284, 1146–1150.

Burns, J.A., Simonelli, D.P., Showalter, M.R., Hamilton, D.P., Porco, C.D., Throop, H., Esposito, L.W., 2004. Jupiter's ring–moon system. In: Bagenal, F., Dowling, T.E., McKinnon, W.B. (Eds.), Jupiter. Cambridge Univ. Press, New York, pp. 241–262.

Charnoz, S., Brahic, A., Thomas, P.C., Porco, C.C., 2007. The equatorial ridges of Pan and Atlas: Terminal accretionary ornaments? Science 318, 1622–1624.

Chenette, D.L., Stone, E.C., 1983. The Mimas ghost revisited—An analysis of the electron flux and electron microsignatures observed in the vicinity of Mimas at Saturn. J. Geophys. Res. 88, 8755–8764.

Cooper, N.J., Murray, C.D., Evans, M.W., Beurle, K., Jacobson, R.A., Porco, C.C., 2008. Astrometry and dynamics of Anthe (S/2007 S 4), a new satellite of Saturn. Icarus 195, 765–777.

Cuzzi, J.N., Burns, J.A., 1988. Charged particle depletion surrounding Saturn's F ring—Evidence for a moonlet belt? Icarus 74, 284–324.

de Pater, I., Gibbard, S.G., Chiang, E., Hammel, H.B., Macintosh, B., Marchis, F., Martin, S.C., Roe, H.G., Showalter, M., 2005. The dynamic neptunian ring arcs: Evidence for a gradual disappearance of Liberté and resonant jump of Courage. Icarus 174, 263–272.

Goldreich, P., Tremaine, S., Borderies, N., 1986. Towards a theory for Neptune's arc rings. Astron. J. 92, 490–494.

Hedman, M.M., Burns, J.A., Tiscareno, M.S., Porco, C.C., Jones, G.H., Roussos, E., Krupp, N., Paranicas, C., Kempf, S., 2007. The source of Saturn's G ring. Science 317, 653–657.

Jones, G.H., Roussos, E., Krupp, N., Beckmann, U., Coates, A.J., Crary, F., Dandouras, I., Dikarev, V., Dougherty, M.K., Garnier, P., Hansen, C.J., Hendrix, A.R., Hospodarsky, G.B., Johnson, R.E., Kempf, S., Khurana, K.K., Krimigis, S.M., Krüger, H., Kurth, W.S., Lagg, A., McAndrews, H.J., Mitchell, D.G., Paranicas, C., Postberg, F., Russell, C.T., Saur, J., Seiß, M., Spahn, F., Srama, R., Strobel, D.F., Tokar, R., Wahlund, J.-E., Wilson, R.J., Woch, J., Young, D., 2008. The dust halo of Saturn's largest icy moon, Rhea. Science 319, 1380–1384.

Kerr, R.A., 2008. Rings around Rhea? Science 319, 1325.

Murray, C.D., Beurle, K., Cooper, N.J., Evans, M.W., Williams, G.A., Charnoz, S., 2008. The determination of the structure of Saturn's F ring by nearby moonlets. Nature 453, 739–744.

Namouni, F., Porco, C., 2002. The confinement of Neptune's ring arcs by the moon Galatea. Nature 417, 45–47.

Porco, C.C., 1991. An explanation for Neptune's ring arcs. Science 253, 995–1001.

Porco, C.C., West, R.A., Squyres, S., McEwen, A., Thomas, P., Murray, C.D., Delgenio, A., Ingersoll, A.P., Johnson, T.V., Neukum, G., Veverka, J., Dones, L., Brahic, A., Burns, J.A., Haemmerle, V., Knowles, B., Dawson, D., Roatsch, T., Beurle, K., Owen, W., 2004. Cassini imaging science: Instrument characteristics and anticipated scientific investigations at Saturn. Space Sci. Rev. 115, 363–497.

Porco, C.C., and the Cassini Imaging Team, 2006a. Rings of Saturn (R/2006 S 1, R/2006 S 2, R/2006 S 3, R/2006 S 4). IAU Circ. 8759, 1.

Porco, C.C., Helfenstein, P., Thomas, P.C., Ingersoll, A.P., Wisdom, J., West, R., Neukum, G., Denk, T., Wagner, R., Roatsch, T., Kieffer, S., Turtle, E., McEwen, A., Johnson, T.V., Rathbun, J., Veverka, J., Wilson, D., Perry, J., Spitale, J., Brahic, A., Burns, J.A., DelGenio, A.D., Dones, L., Murray, C.D., Squyres, S., 2006b. Cassini observes the active south pole of Enceladus. Science 311, 1393–1401.

Porco, C.C., Thomas, P.C., Weiss, J.W., Richardson, D.C., 2007. Saturn's small inner satellites: Clues to their origins. Science 318, 1602–1607.

Porco, C.C., on behalf of the Cassini Imaging Team, 2008. R/2006 S 5 and R/2007 S 1. IAU Circ. 8970.

Roussos, E., Jones, G.H., Krupp, N., Krimigis, S.M., Mitchell, D., Paranicas, C., 2006. R/2006 S 5. IAU Circ. 8773, 3.

Roussos, E., Jones, G.H., Krupp, N., Paranicas, C., Mitchell, D.G., Krimigis, S.M., Woch, J., Lagg, A., Khurana, K., 2008. Energetic electron signatures of Saturn's smaller moons: Evidence of an arc of material at Methone. Icarus 193, 455–464.

Showalter, M.R., Lissauer, J.J., 2006. The second ring–moon system of Uranus: Discovery and dynamics. Science 311, 973–977.

Showalter, M.R., Cheng, A.F., Weaver, H.A., Stern, S.A., Spencer, J.R., Throop, H.B., Birath, E.M., Rose, D., Moore, J.M., 2007. Clump detections and limits on moons in Jupiter's ring system. Science 318, 232–234.

Showalter, M.R., de Pater, I., Verbanac, G., Hamilton, D.P., Burns, J.A., 2008. Properties and dynamics of Jupiter's gossamer rings from Galileo, Voyager, Hubble and Keck images. Icarus 195, 361–377.

Spitale, J.N., Jacobson, R.A., Porco, C.C., Owen Jr., W.M., 2006. The orbits of Saturn's small satellites derived from combined historic and Cassini imaging observations. Astron. J. 132, 692–710.

van Allen, J.A., 1983. Absorption of energetic protons by Saturn's ring G. J. Geophys. Res. 88, 6911–6918.